İSTANBUL UNIVERSITY
CERRAHPAŞA

ORIGINAL ARTICLE
Electrica 2024; 24(1): 210-217

Frequency Response Analysis of MEMS Comb-Drive Resonator Integrated With a Polymer Thin Film Layer

Serdar Tez[1], **Mehmet Kaya**[2]

[1]Department of Electrical and Electronics Engineering, Pamukkale University Faculty of Engineering, Denizli, Turkey
[2]Pamukkale University The Graduate School of Natural and Applied Sciences, Electrical-Electronics Engineering, Denizli, Turkey

Cite this article as: S. Tez and M. Kaya, "Frequency response analysis of MEMS comb-drive resonator integrated with A polymer thin film layer," *Electrica*, 24(1), 210-217, 2024.

ABSTRACT

This paper presents a finite element method (FEM) simulation study for micro-electro-mechanical systems capacitive comb-finger resonator. The designed resonator is conceptually integrated with a 0.75 µm-thick sensing layer poly(3,4-ethylenedioxythiophene), which is necessary to detect volatile organic chemicals (VOCs). The rest capacitance and resonance frequency values are determined with FEM simulations for coated and uncoated devices. Moreover, the conductance and the equivalent parallel capacitance of the sensors are examined with respect to the frequency by considering variables such as the quality factor and applied potential. The die size of the designed resonator is approximately 1770 µm × 2000 µm × 35 µm, and the theoretically calculated mass responsivity of the resonator is nearly 8.8 pg/Hz. We think that the proposed resonator structure can have potential use in the detection of VOCs.

Index Terms— Capacitive resonator, Finite element method (FEM), Frequency response, Mass sensor, Micro-electro-mechanical systems (MEMS)

I. INTRODUCTION

Micro-electro-mechanical systems (MEMS) resonators have found a place in several implementations in various research interests such as timing, frequency control [1], and filtering [2] as well as sensing applications [3]. Within sensing applications, mass sensors are one of the well-known ones depending on the method of the resonant frequency shift. On the other hand, resonant mass sensors generally need a sensing layer to interact with the biological or chemical samples intended to be detected, resulting in resonance frequency shifts as a result of added mass. Therefore, the cantilever or clamped-clamped beam resonator structures are generally preferred in resonant mass sensing applications for their simple form, and they can be more easily integrated with the sensing layers without losing their functionality by using different deposition methods [4-7]. Moreover, MEMS comb-drive resonator structures have been used in resonant mass sensing applications [8-11] as some drawbacks have been observed in the performance of the cantilevers [8]. On the other hand, the main problem in these implementations is the integration of the sensing layer on the mass sensor due to the complex structure of the comb-drive resonator. There are several ideas and solutions for this situation in the literature. One of them is to deposit sensing material on a microcantilever-type mass sensor driven by the comb drive actuation with inkjet printing [7,10]. The other one is to use a spray coating given in [9]. On the other hand, the number of sensing elements used with the spray coating is limited, and the necessity of utilizing a shadow mask as well as alignment with the sensor are introduced as extra steps for the fabrication process for this idea. Moreover, it requires a high-volume consumption of sensing elements during the coating processing. Therefore, a more efficient way for the integration of the sensing element with the mass sensor is introduced in [11] by using the electropolymerization method.

The frequency response is one of the elemental interests affecting the dynamic behavior of the resonator structures. Moreover, for the functionality test of the mass sensor, one of the main concerns is to estimate the resonance frequency of the resonator after the integration of the sensing layer. Therefore, there are several studies focusing on the frequency response of the cantilever structure [12,13]. On the other hand, a limited number of studies [14,15] were performed for the MEMS comb drive resonator.

Corresponding author:
Serdar Tez

E-mail:
stez@pau.edu.tr

Received: August 04, 2023

Accepted: November 21, 2023

Publication Date: January 31, 2024

DOI: 10.5152/electrica.2024.23124

Content of this journal is licensed under a Creative Commons Attribution-NonCommercial 4.0 International License.

The main purpose of this study is to conceptually design and simulate a sensor which is dependent on the resonant frequency shift. Therefore, the resonance frequency of a designed MEMS comb-drive resonator integrated with a sensing layer is investigated by using the finite element simulation method. The selected sensing element is poly(3,4-ethylenedioxythiophene) (PEDOT), and its absorbing and swelling features resulting in mass change can be used for sensing mechanism [16] in the detection of volatile organic chemicals (VOCs) [16-17], which are biomarkers for certain diseases and threaten indoor air quality [17]. Furthermore, the PEDOT layer as a conducting polymer can also be integrated with the MEMS comb-drive resonator structure by using a method given in [11]. The frequency response of the proposed structure is simulated by considering variables such as the quality factor (Q) and the applied voltage. Furthermore, the conductance and the equivalent parallel capacitance of the resonator structures are also simulated by using finite element method (FEM) data with the theoretical background already given in the literature. Moreover, this study can be further improved by simulating the absorbing and swelling behavior of the polymer layer at the molecular level in the presence of VOCs, resulting in mass change.

II. DESIGN

Figure 1 illustrates the structure of the MEMS resonator. The structural thickness is selected as 35 µm during the design study. There are two mechanical springs of which one side is attached to the proof mass part of the sensor while the other side is fastened to the anchor region. The dimensions of the mechanical spring structure are 50 µm in length and 4 µm in width. With this placement of the mechanical spring structures, the MEMS resonator structure moves in-plane direction. On the other hand, the undesired vertical movement of the proof mass structure is hindered by the relatively high spring constant in the out-of-plane direction. The number of capacitive fingers mutually placed among the proof mass and the anchor regions are 19. The overlap length for the capacitive finger is 60 µm in length, and the capacitive gap is 2 µm. Some of the theoretical calculations are performed by using the expressions and material features already given in the literature [18-19] for MEMS comb-drive resonators, and the design parameters are summarized in Table I, where the material properties of silicon having <111> crystal orientation is taken into account.

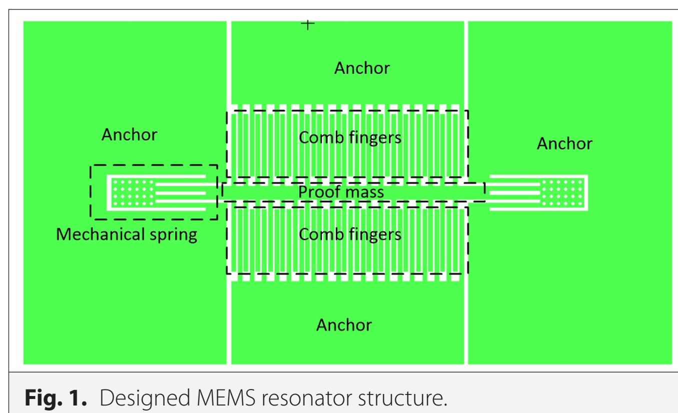

Fig. 1. Designed MEMS resonator structure.

TABLE I. THE DESIGN PARAMETERS OF THE PRESENTED MEMS RESONATOR STRUCTURE

Parameters	Design Values
Structural thickness (µm)	35
Spring width (µm)	4
Spring length (µm)	50
Number of mechanical springs	2
Spring constant (N/m)	6057
Finger width (µm)	4
Finger length (µm)	70
Overlap finger length	60
Capacitive gap (µm)	2
Capacitive anti-gap (µm)	2
Number of the capacitive finger per side	19
Proof mass amount (kg)	1.44×10^{-9}
Resonance frequency (kHz)	325.750
Rest capacitance (F)	3.43×10^{-13}
Effective sensitivity (ạC/ạx) (F/m)	5.73×10^{-9}
Mass responsivity (pg/Hz)	8.8

III. SIMULATION STUDY FOR FUNCTIONALIZED MASS SENSOR WITH PEDOT

The confirmation of the design parameters is provided by using ELMER FEM an open-source finite element analysis software [20]. The two different three-dimensional models of the designed resonator are formed by utilizing FreeCAD, a computer-aided design (CAD) [21] software for uncoated and coated resonator structures. During the formation of the conceptual design, the modified silicon on glass fabrication process of which process details given in [22-25] is considered. On the other hand, the silicon-on-insulator-based fabrication process can be also considered for the proposed structure [26]. Figure 2 depicts a conceptual design of the resonator integrated with a PEDOT, where the integration of sensing material can be performed with a method given in [11].

While simulating the designed resonator structure integrated with PEDOT, the PEDOT material properties presented in [27-28] are considered. Then, first, the modal analysis is completed on not only uncoated device but also on coated resonator structure with a 0.75-µm thick PEDOT layer. The obtained simulation results from ELMER FEM are visualized by using ParaView software [29]. Furthermore, the formed capacitance value is also simulated. For this simulation, another CAD formation is considered for the region among the fingers. Then, this 3D model is simulated with ELMER FEM by applying a potential to the boundary region for the air medium, and the capacitance value is calculated as 0.41 pF. Figure 3 illustrates the results of the modal analysis and the rest capacitance calculation performed with ELMER FEM and visualized with ParaView software. It should be noted that the obtained result is highly different from that of the

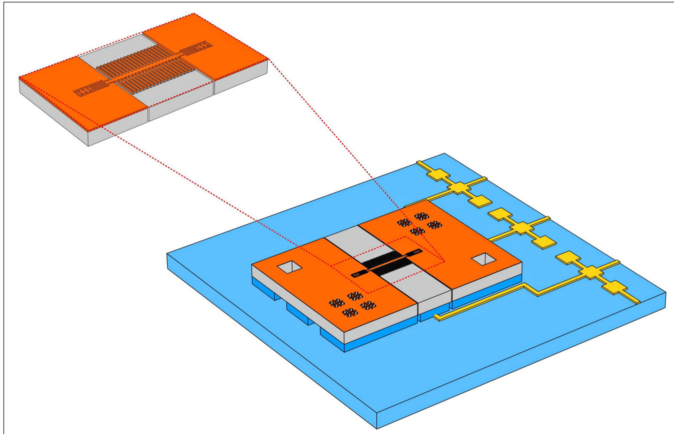

Fig. 2. The conceptual model of the designed MEMS resonator after the integration. The orange color indicates the 0.75 μm-thick PEDOT layer.

theoretical calculation for the resonance frequency. The reason for this can be explained by the effective mass of the resonator which is the whole moving-proof mass having a highly small size. On the other hand, the slight difference observed in the capacitance value between the simulation and theoretical calculation is attributed to the fringing field.

As the main purpose is to determine the resonance frequency and frequency response of the MEMS resonator after the integration of the sensing layer, the finite element analysis simulation study is performed. There are several studies focusing on the frequency response of the resonator by using the FEM method [14, 30]. The same approach defined in [14,30] is used to simulate the frequency response of the proposed structure with Elmer FEM. Thus, the simulation study is performed by considering the parameters affecting the dynamic behavior of the resonator. The theoretical model of the MEMS resonator structures can be given with a mass-spring-damper system of which the dynamic behavior is given with the following Eq. (1) [18]

$$\frac{X(s)}{F(s)} = \frac{1}{ms^2 + bs + k} \tag{1}$$

where X is the displacement, F is the electrostatic force, b is the damping coefficient, k is the spring constant, and m is the proof mass amount. As seen, the displacement is closely related to electrostatic force and damping coefficient. The electrostatic force equation can also be defined with the following equation:

$$\mathbf{F} = \frac{1}{2}\frac{\partial C}{\partial x}V^2 \quad ((2)$$

where V is the electrical potential including AC and DC terms, and C is the capacitance. Furthermore, the quality factor can also be expressed with respect to the angular resonance frequency (ω_0) and damping coefficient (b) with the following equation:

$$Q = \frac{\omega_0 m}{b} \tag{3}$$

where the angular resonance frequency can be given with the following expression:

$$\omega_0 = \sqrt{\frac{k}{m}} \tag{4}$$

When the beforementioned equations are examined, it can be observed that there are two main factors influencing the dynamic characteristic of the resonator which are the quality factor and applied potential. Therefore, during the simulation study, not only

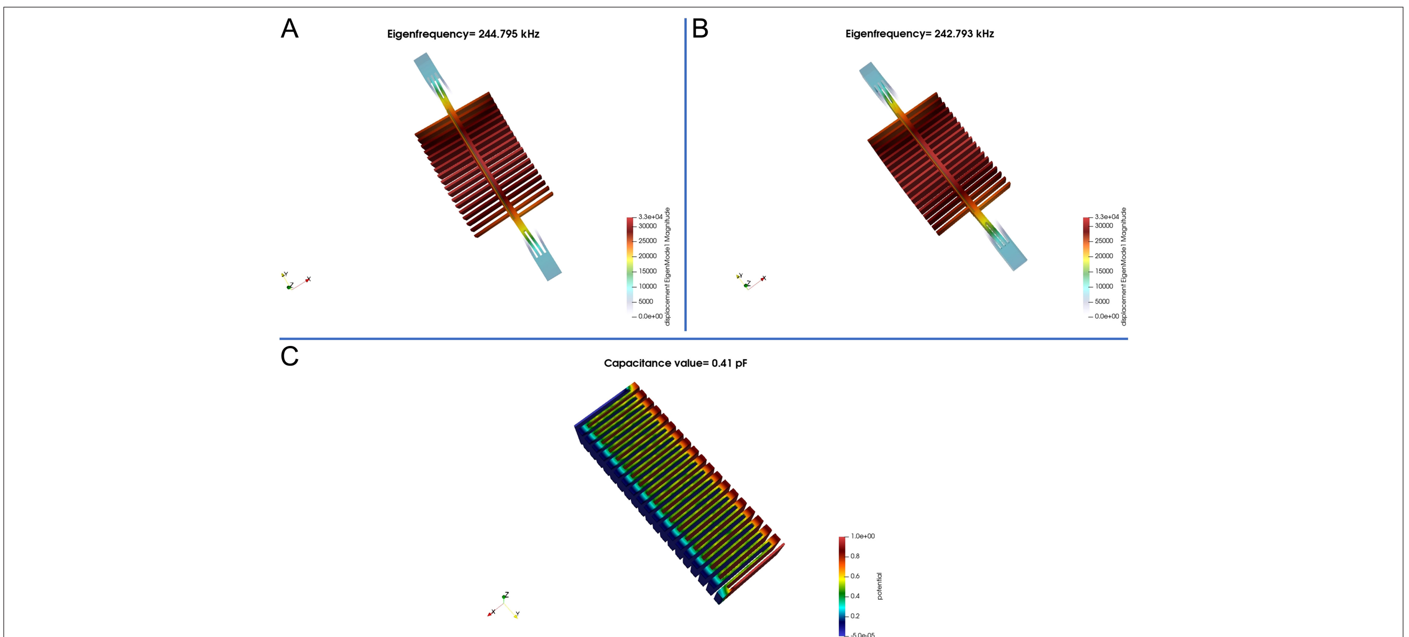

Fig. 3. Elmer FEM modal analysis results illustrating the first mechanical mode, (a) for uncoated resonator (244.795 kHz) and (b) for coated resonator (242.793 kHz). (c) The formed rest capacitance value is 0.41 pF.

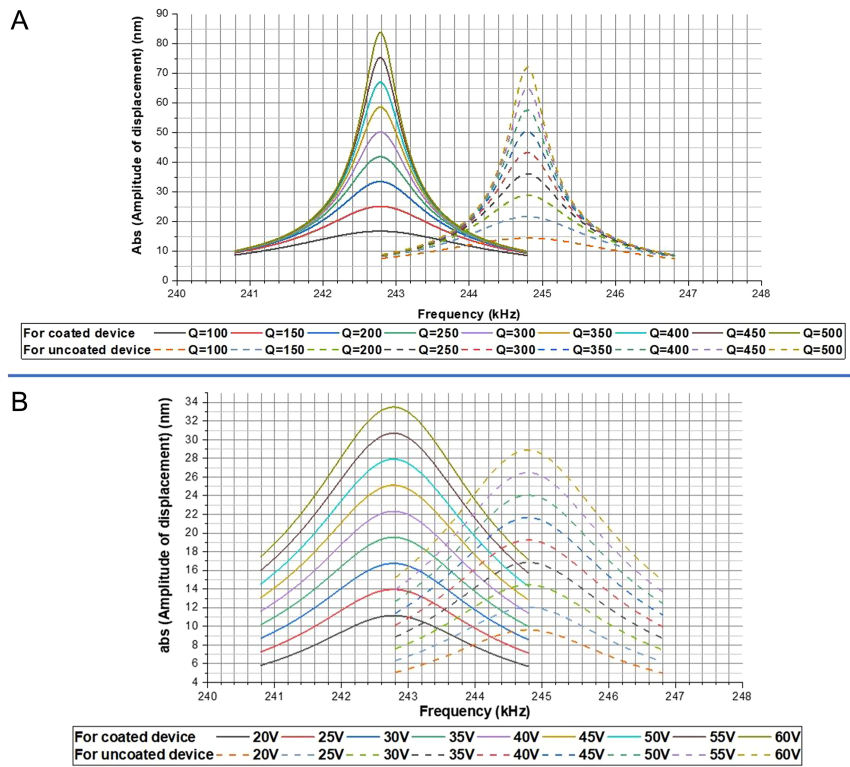

Fig. 4. Frequency response analysis for the designed MEMS resonator for coated and uncoated devices. (a) With respect to the quality factor for the applied DC potential 30 V and AC 2 V level. (b) With respect to the applied DC potential for Q = 100 and fixed AC 2 V level.

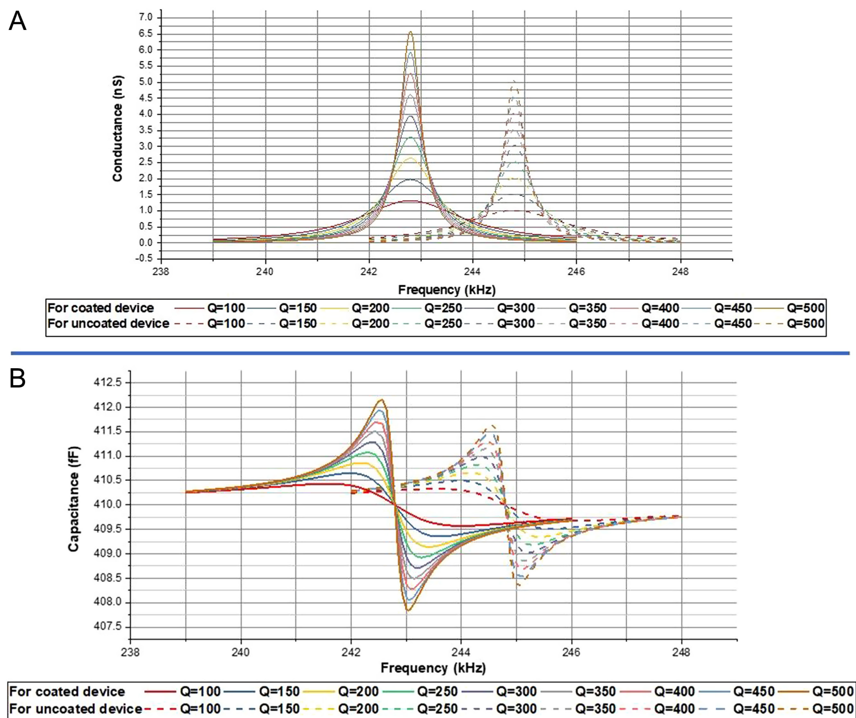

Fig. 5. (a) Conductance vs frequency for the designed MEMS resonator. (b) Capacitance vs frequency for the designed MEMS resonator with respect to the quality factor for the fixed 30 V DC and AC 2 V level for coated and uncoated devices.

quality factor but also applied potential are selected as variables. The Rayleigh damping model is considered to model the damping mechanism for the proposed structure [31]. As the resonator is considered to operate in atmosphere pressure, the quality factor is swept for different values during the simulation. Figure 4 shows the results of the frequency analysis. The resonance frequency for the proposed structure is the frequency where the amplitude has a maximum value. As expected, when the quality factor value increases for the applied fixed 30 V DC potential and AC 2 V level, an increment in the amplitude of the displacement value is also observed in Fig. 4 (a) for the uncoated and coated devices. On the other hand, the amplitude of the displacement increases with respect to the applied DC potential with a fixed AC 2 V level for coated and uncoated resonator structures considering a fixed Q = 100 value, which can be also observed in Fig. 4 (b). Also, it should be noted that the amplitude of the displacement at the resonance frequency can also be used to estimate the motional current value.

The electrical equivalent circuit of the MEMS resonator near the resonance frequency is given, and the theoretical background is discussed in [32]; where the conductance and the equivalent parallel capacitance expressions are defined using the following equations [32]:

$$G(\omega)=\frac{R_m}{R_m^2+\left(\omega L_m-\frac{1}{\omega C_m}\right)^2} \tag{5}$$

$$C_{eq}=\frac{B(\omega)}{\omega}=C_0+C_{stray}+L_m\frac{\frac{\omega_0^2}{\omega^2}-1}{R_m^2+\left(\omega L_m-\frac{1}{\omega C_m}\right)^2} \tag{6}$$

where $G(\omega)$, C_{eq} and $B(\omega)$ are the conductance, the equivalent capacitance, and susceptance, respectively. Furthermore, C_0 and C_{stray} are the static capacitance and the parasitic capacitance, respectively. Moreover, R_m, L_m, and C_m are the motional parameters to use the model of the MEMS resonator, and they can be defined as motional resistance, motional inductance, and motional capacitance, respectively. Their equations are defined as the following:

$$L_m=\frac{m}{\eta^2} \tag{7}$$

$$R_m=\frac{b}{\eta^2} \tag{8}$$

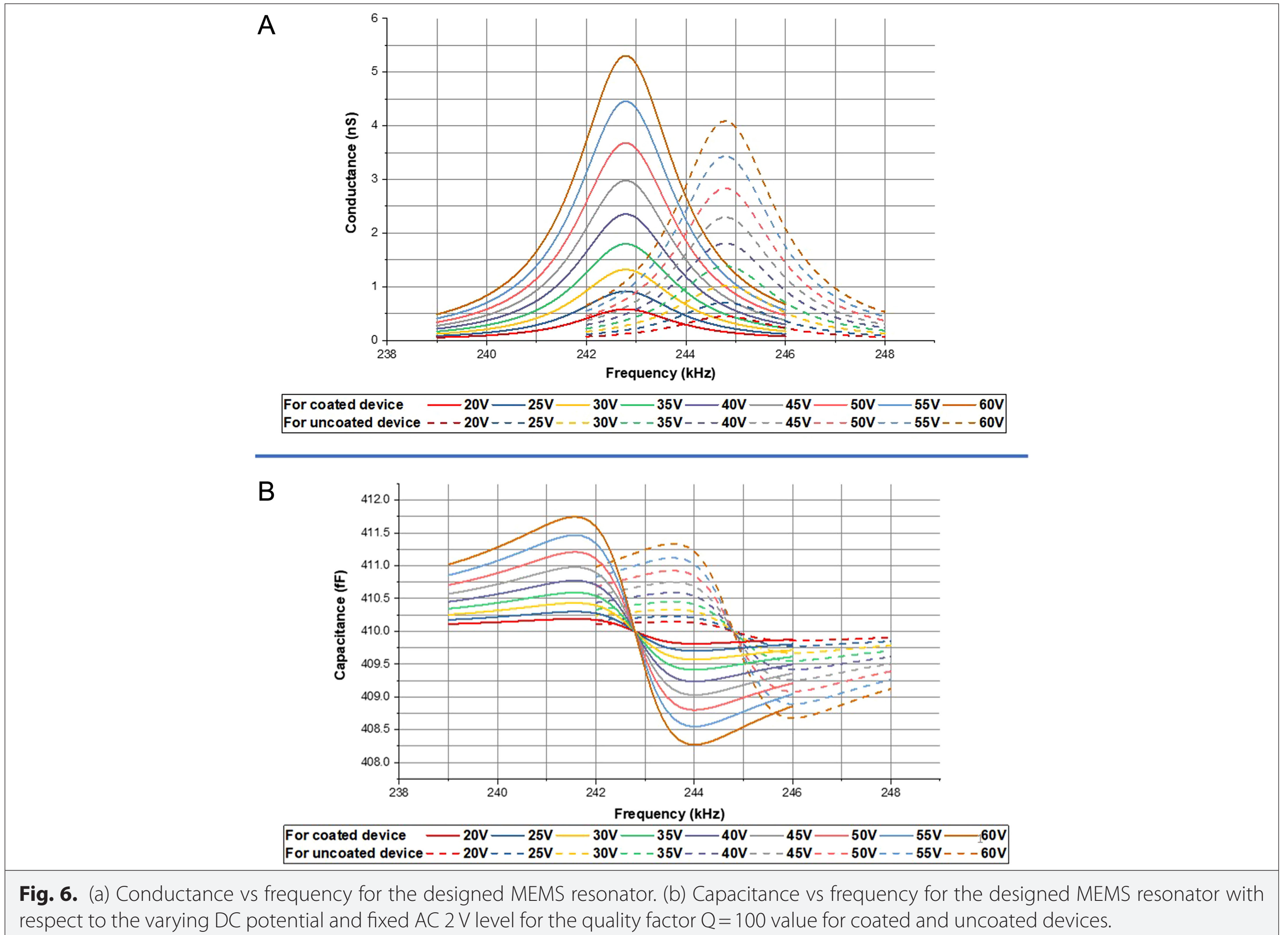

Fig. 6. (a) Conductance vs frequency for the designed MEMS resonator. (b) Capacitance vs frequency for the designed MEMS resonator with respect to the varying DC potential and fixed AC 2 V level for the quality factor Q = 100 value for coated and uncoated devices.

$$C_m = \frac{\eta^2}{k} \tag{9}$$

where η denotes to the electromechanical coupling coefficient constant, and its equation is

$$\eta = \frac{\partial C(x)}{\partial x} \times V_{DC} \tag{10}$$

Elmer FEM is able to calculate the electrostatic force, and η can be obtained by using Eq. (2) and the applied potential. This value is also utilized to calculate the motional parameters R_m, L_m, and C_m. Thus, the conductance and the equivalent parallel capacitance value can be calculated with Elmer FEM data by using Eqs. (5-6). The obtained graphs for the conductance and the equivalent capacitance with respect to the frequency are given in Figs. 5 and 6 for the variables such as the quality factor and the DC potential. When Fig. 5 and 6 are examined, the conductance and the equivalent parallel capacitance value are slightly higher than that of the uncoated device in both cases. The reason for this can be related to the fringing field as the PEDOT layer is taken into account as 0.75 µm during the simulation study. Furthermore, as our model only comprise the coating on the proof mass for simplicity, it is expected that the obtained simulation values for the capacitance will slightly differ from the functionality test result of the fabricated device. A more realistic approach can be simulated by considering the PEDOT layer for regions among the capacitive gap, at the expense of increasing computational duration and meshing a more complex 3D model for FEM analysis. The effect of a polymer integration on the capacitance of the comb-drive resonator can be observable in experimental results given in [11].

IV. CONCLUSION

This study conceptually proposes a MEMS comb-finger structure integrated with a PEDOT polymer layer. The frequency response of the proposed resonator is performed by using Elmer FEM for the different values of the quality factor and the DC voltage values as the proposed device is planned to operate under atmosphere pressure. During the simulations, the maximum value of the amplitude of the displacement is determined for the frequency, which equals the resonance frequency. This value can also be used to determine the motional current value. Furthermore, the functionality test of the sensor can be planned to perform by using an LCR meter after the fabrication; therefore, the parallel plate equivalent capacitance and the conductance values are also obtained with respect to the frequency by using the data obtained from the results of the FEM simulations. The obtained results only show the resonator structure frequency response after the integration of the polymer film. On the other hand, this study can be further improved by simulating PEDOT mass change at the molecular level in the presence of VOCs. Although the current study focuses on the integration MEMS resonator with a polymer layer to detect VOCs, it is also possible to broaden this study with the different sensing elements for the different biological species and various chemical analytes.

Peer-review: Externally peer-reviewed.

Author Contributions: Concept – S.T., M.K.; Design – S.T., M.K.; Supervision – S.T.; Funding – TUBITAK 116E231.; Materials – S.T., M.K.; Data Collection and/or Processing – S.T., M.K.; Analysis and/or Interpretation – S.T., M.K.; Literature Review – S.T., M.K.; Writing – S.T., M.K.; Critical Review – S.T., M.K.

Declaration of Interests: The authors have no conflict of interest to declare.

Funding: This study is supported by the Scientific and Technological Research Council of Turkey (TUBITAK) under the grant number 116E231. The authors would like to thank TUBITAK.

REFERENCES

1. C. T. C. Nguyen, "MEMS technology for timing and frequency control," *IEEE Trans. Ultrason. Ferroelectr. Freq. Control*, vol. 54, no. 2, pp. 251–270, February 2007. [CrossRef]
2. L. Lin, R. T. Howe, and A. P. Pisano, "Microelectromechanical filters for signal processing," *J. Microelectromech. Syst.*, vol. 7, no. 3, pp. 286–294, 1998. [CrossRef]
3. G. S. Wood, C. Zhao, S. H. Pu, S. A. Boden, I. Sari, and M. Kraft, "Mass sensor utilising the mode-localisation effect in an electrostatically-coupled MEMS resonator pair fabricated using an SOI process", *Microelectronic Engineering*. vol. 159, pp. 169–173, 2016. [CrossRef]
4. B. Guruprasad, and M. G. Veena, "Analysis of MEMS cantilever sensor for sensing volatile organic compounds," *Micro Nano Eng.*, vol. 16, p. 100143, 2022. [CrossRef]
5. N. Jaber, S. Ilyas, O. Shekhah, M. Eddaoudi, and M. I. Younis, "Resonant gas sensor and switch operating in air with metal-organic frameworks coating," *J. Microelectromech. Syst.*, vol. 27, no. 2, pp. 156–163, 2018. [CrossRef]
6. L. N. Quang *et al.*, "Electrochemical pyrolytic carbon resonators for mass sensing on electrodeposited polymers," *Micro Nano Eng.*, vol. 2, pp. 64–69, 2019. [CrossRef]
7. S. S. Bedair, and G. K. Fedder, "Polymer mass loading of CMOS/MEMS microslot cantilever for gravimetric sensing," SENSORS, 2007 IEEE. IEEE Publications, vol. 2007, pp. 1164–1167, 2007. [CrossRef]
8. E. Bayraktar, D. Eroglu, A. T. Ciftlik, and H. Kulah, "A MEMS based gravimetric resonator for mass sensing applications.", IEEE 24th International Conference on Micro Electro Mechanical Systems, Cancun, Mexico, 2011, pp. 817–820. [CrossRef]
9. S. Tez, and E. Aytaşkın. "Design of a MEMS-Based Capacitive Resonator for Target Analyte Detection," *Electrica*, vol. 20, no. 1, pp. 41-51, 2020.
10. K. L. Dorsey, S. S. Bedair, and G. K. Fedder, "Gas chemical sensitivity of a CMOS MEMS cantilever functionalized via evaporation driven assembly," *J. Micromech. Microeng.*, vol. 24, no. 7, p. 075001, 2014. [CrossRef]
11. S. Tez, and M. Ak. "Integration of conducting polymers with MEMS lateral comb-drive resonator via electrodeposition for VOCs detection," *J Mater Sci* vol. 58, pp. 3078–3093, 2023. [CrossRef]
12. M. Shoaib, N. Hisham, N. Basheer, and M. Tariq, "Frequency and displacement analysis of electrostatic cantilever-based MEMS sensor," *Analog Integr. Circ. Sig Process*, vol. 88, no. 1, pp. 1–11, 2016. [CrossRef]
13. I. S. Amiri, and S. Addanki, "Simulation fabrication and characterization of micro-cantilever array based ozone sensor," *Results Phys.*, vol. 10, pp. 923–933, 2018. [CrossRef]
14. S. Tez, and M. Kaya, "A simulation study verified by experimental test results for frequency response analysis of MEMS comb-drive resonator," *Microsyst Technol.*, 2023. [CrossRef]
15. N. Khan, and M. J. Ahamed, "Design and development of a MEMS butterfly resonator using synchronizing beam and out of plane actuation," *Microsyst. Technol.*, vol. 26, no. 5, pp. 1643–1652, 2020. [CrossRef]
16. J. N. Gavgani et al., "A room temperature volatile organic compound sensor with enhanced performance, fast response and recovery based on N-doped graphene quantum dots and poly(3,4-ethylenedioxythiophene)–poly(styrenesulfonate) nanocomposite," *RSC Adv.*, vol. 5, no. 71, p. 57559–57567, 2015. [CrossRef]
17. M. Tomić, M. Šetka, L. Vojkůvka, and S. Vallejos, "VOCs sensing by metal oxides, conductive polymers, and carbon-based materials," *Nanomaterials (Basel)*, vol. 11, no. 2, p. 552, 2021. [CrossRef]
18. R. Abdolvand, B. Bahreyni, J. E. Lee, and F. Nabki, "Micromachined Resonators: A Review" *Micromachines*, vol. 7, no. 9, p. 160, 2016. [CrossRef]
19. M. A. Hopcroft, W. D. Nix, and T. W. Kenny, "What is the Young's modulus of silicon?," *J. Microelectromech. Syst.*, vol. 19, no. 2, pp. 229–238, 2010. [CrossRef]
20. P. Råback, M. Malinen, J. Ruokolainen, A. Pursula, and T. Zwinger, Eds., "Elmer models manual," CSC–IT Center for Science, 2019. Available: http://www.nic.funet.fi/pub/sci/physics/elmer/doc/ElmerModelsManual.pdf

21. J. Riegel, W. Mayer, and Y. Havre. *FreeCAD, version 0.18.4r*, 2021. Available: http://www.freecadweb.org. Accessed 31/07/2023.
22. M. M. Torunbalci, E. Tatar, S. E. Alper, and T. Akin, "Comparison of two alternative silicon-on-glass microfabrication processes for MEMS inertial sensors", *Eurosensors*, Vol. XXV, pp. 900–903, 2011.
23. S. Tez, U. Aykutlu, M.M. Torunbalci, and T. Akin. "A Bulk-Micromachined Three-Axis Capacitive MEMS Accelerometer on a Single Die," *J. Microelectromechanical Syst*. vol. 24, pp. 1264–1274, 2015. [CrossRef]
24. S. Tez, and T. Akin. "Fabrication of a sandwich type three axis capacitive MEMS accelerometer," *SENSORS, 2013 IEEE*, Baltimore, MD, USA, pp. 1-4, 2013. [CrossRef]
25. S. Tez, and T. Akin. "Comparison of Two Alternative Fabrication Processes for a Three-Axis Capacitive MEMS Accelerometer," *Procedia Eng*. Vol. 47 pp. 342–345, 2012. [CrossRef]
26. I. Sari, I. Zeimpekis, and M. Kraft, "A dicing free SOI process for MEMS devices," *Microelectron. Eng.*, vol. 95, pp. 121–129, 2012. [CrossRef]
27. A. Lenz, H. Kariis, A. Pohl, P. Persson, and L. Ojamäe, "The electronic structure and reflectivity of PEDOT:PSS from density functional theory," *Chem. Phys.*, vol. 384, No. 1–3, pp. 44–51, 2011. [CrossRef]
28. J. Qu, Liangqi Ouyang, C.-C. Kuo, and D. C. Martin, "Stiffness, strength and adhesion characterization of electrochemically deposited conjugated polymer films," *Acta Biomater.*, vol. 31, pp. 114–121, 2016. [CrossRef]
29. J. Ahrens, B. Geveci, and C. Law, *Paraview: An End-User Tool for Large Data Visualization, Visualization Handbook*, 1st edn, Amsterdam: Elsevier, 2005, pp. 717–731.
30. S. Tez, and M. Kaya. "Development of algorithms in open-source Elmer FEM for frequency response and biased modal analysis of MEMS cantilever," *J Comput Electron* Vol. 20, pp. 1020–1031, 2021. [CrossRef]
31. M. Liu, and D. G. Gorman, "Formulation of Rayleigh damping and its extensions," *Comput. Struct.*, vol. 57, No. 2, pp. 277–285, 1995. [CrossRef]
32. Y. Sabry, M. Medhat, B. Saadany, T. Bourouina, and D. Khalil, "Parameter extraction of MEMS comb-drive near-resonance equivalent circuit: Physically-based technique for a unique solution," *J. Micro/Nanolith. MEMS MOEMS*, vol. 11, no. 2, 2012. [CrossRef]

Serdar Tez received the B.S and the M.S. degrees in the Physics Department from the Süleyman Demirel University, Isparta, Turkey, in 2004 and 2006, respectively. He joined the METU-MEMS Research and Applications Center in 2008. He received the Ph.D. degree in the Micro and Nanotechnology Graduate Program from the Middle East Technical University (METU), Ankara, Turkey, in 2014, with the work on MEMS capacitive three-axis accelerometers. Currently, he is with the Department of Electrical and Electronics Engineering, Pamukkale University, Denizli, 20070 Turkey. His current research interests are the design, simulation, and fabrication methods of microstructures.

Mehmet Kaya received the B.S. degree in the Department of Electrical and Electronics Engineering from Pamukkale University, Denizli, Turkey, in 2018. Currently, he is a graduate student in the Department of Electrical and Electronics Engineering, Graduate School of Natural and Applied Sciences at Pamukkale University. He works on MEMS Capacitive Sensors. His research interests are the design, simulation, and modeling of microsensors and micro actuators.